Stochastic star formation in the Milky Way inferred from the unity index of KS law

Yoshiaki SOFUE[1]

[1]Institute of Astronomy, The University of Tokyo, Mitaka, Tokyo 186-0015, Japan

*E-mail: sofue@ioa.s.u-tokyo.ac.jp

Abstract

We performed a correlation analysis between the brightness temperature of the CO line and number density of HII regions in the longitude-velocity diagram (LVD) of the Milky Way in order to investigate the volumetric star-formation law. We determined the index α of the Kennicut-Schmidt law for the molecular gas defined by $\rho_{\mathrm{SFR}} \propto \rho_{\mathrm{H_2}}^{\alpha}$, where ρ_{SFR} is the SFR (star-formation rate) density and $\rho_{\mathrm{H_2}}$ is the molecular gas density. We obtained $\alpha = 1.053 \pm 0.075$ and 1.031 ± 0.067 for the CO-line data from the Nobeyama 45-m and Columbia 1.2-m telescope Galactic plane surveys, respectively. This result is consistent with the KS indices currently determined for the molecular gas in the Milky Way as well as in spiral and starburst galaxies. We argue that an index close to 1 is universal in favor of stochastic (spontaneous) star formation, but is inconsistent with cloud collision model that predicts a steeper index of $\alpha = 2$. We also suggest that the efficiency of star formation in the Galactic Centre is an order of magnitude lower than that in the disc.

Key words: Galaxy: evolution — ISM: HII regions — ISM: clouds — ISM: molecules — stars: formation

1 Introduction

The trigger of star formation (SF) in the molecular clouds in the Galaxy has been one of the fundamental subjects of the ISM over the decades (Shu et al. 1987; Lada & Lada 2003). There appear two major ideas: one scenario is the stochastic (spontaneous) SF by self-regulation mechanisms in individual molecular clouds due to the gravitational instability and/or sequential compression by expanding shells of HII regions (Elmegreen & Lada 1977; Myers 2009; Hacar et al. 2023; Pineda et al. 2023). Another scenario is the external triggering by collisions of molecular clouds (Habe & Ohta 1992; Hasegawa et al. 1994; Kimura & Tosa 1996; Fukui et al. 2021).

A possible way to clarify the SF mechanisms is to check the index α of the Kennicutt-Schmidt (KS) law (Kennicutt & Evans 2012) defined through

$$\rho_{\mathrm{SFR}} = A \, (\rho_{\mathrm{H_2}})^{\alpha}, \tag{1}$$

where ρ_{SFR} $[M_{\odot} \, \mathrm{y}^{-1} \, \mathrm{kpc}^{-3}]$ and $\rho_{\mathrm{H_2}}$ $[\mathrm{H_2} \, \mathrm{cm}^{-3}]$ are the volumetric densities of SFR and the molecular gas, respectively, and A is a constant. The stochastic SF predicts $\alpha = 1$, because ρ_{SFR} is proportional to the density of the clouds, whereas the collision process requires $\alpha = 2$, because ρ_{SFR} depends on the collision frequency among the clouds. The current measurements have shown $\alpha \sim 1$ in the Milky Way (Fuchs et al. 2009; Sofue 2017; Sofue & Nakanishi 2017; Elia et al. 2022) and spiral galaxies (Komugi et al. 2006; Kennicutt & Evans 2012), which indicated SFR density more linearly proportional to the molecular gas density.

The KS law in the Milky Way has been studied using the face-on maps of the molecular and HI gases and of HII regions (Sofue & Nakanishi 2017; Sofue 2017; Spilker et al. 2021; Bacchini et al. 2019; Elia et al. 2022). Recent studies of the face-on transformation (FOT) from the radial velocity to line-of-sight distance have shown that the derived gas distribution is highly sensitive to the rotation curve (RC) (Marasco et al. 2017; Fujita et al. 2023). So, in this paper, we propose a new, simpler and more direct method to derive the KS-law index using the longitude-velocity diagram (LVD) without employing the FOT (Koda et al. 2016). By applying the new method, we determine the KS law index α for the molecular gas, and discuss the feasibility of the stochastic and collision models for the star formation.

In the analysis, we use the archival data of ^{12}CO -line emission from the FUGIN (Four-receiver system Unbiased Galactic plane Imaging survey with the Nobeyama 45-m telescope) (Umemoto et al. 2017), Galactic Centre survey (Tokuyama et al. 2019), and Columbia 1.2-m Galactic plane survey (Dame et al. 2001), combined with the WISE
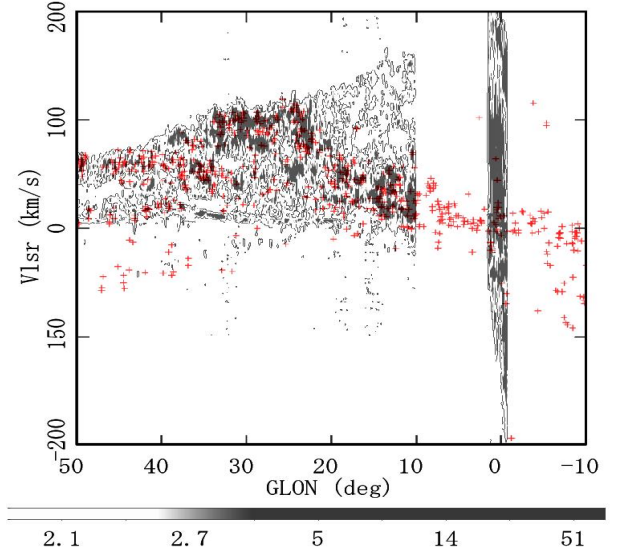

Fig. 1. HII regions in the Galactic plane at $|b| \leq 0^{\circ}.2$ from the WISE catalogue (Anderson et al. 2014) superposed on the LVD of CO-line brightness constructed from the data by the Nobeyama 45-m FUGIN (Umemoto et al. 2017) and GC survey (Tokuyama et al. 2019). The bar indicates T_{B} inK and the contours are drawn at $T_{\mathrm{B}} = 0.5$ K.

(Wide-field Infrared Survey Explore) HII region catalogue (Anderson et al. 2014).

2 Molecular-gas KS law using LVD

We perform correlation analysis on the LVD between the number density of HII regions from the WISE catalogue (Anderson et al. 2014) and the volume density of H_2 molecules calculated from the Nobeyama CO-line surveys (Umemoto et al. 2017; Tokuyama et al. 2019) in the inner disc of the Milky Way. Correlation on the LVD is more directly coupled to the data, bypassing the sophisticated face-on transition procedures Koda et al. 2016. Figure 1 plots longitude-velocity positions of HII regions in the Galactic plane superposed on the CO-line LVDs along the Galactic plane ($b = 0^{\circ}$). As readily known (Hou & Han 2014), HII regions and CO line intensity are tightly correlated in the LVD.

In our study we constrain the region of analysis in the Galactic plane by using only the HII regions in the Galactic plane at $|b| \leq 0^{\circ}.2$ and CO LVD at $b = 0^{\circ}$. The region was so chosen in order to avoid the uncertainty during the determination process of the height from the Galactic plane depending on the distance ambiguity. Thus we selected 492 HII regions, about 38% of the 1316 catalogued sources with measurements of LSR velocities in the radio recombination lines (RRL). We then calculate the number density N of HII regions and CO brightness temperature T_{B} averaged in every (l, v) grid with bin size $\delta l \times \delta v = 0^{\circ}.25 \times 10$

km s^{-1}for Nobeyama and $2° \times 5$ km s^{-1}for Columbia CO survey data.

Using the thus obtained sets of N and T_B, we calculate the volume densities n_i of HII regions ($i = $ HII) and H_2 molecules ($i = H_2$) by

$$n_i = \frac{dN_i}{ds} = \frac{dN_i}{dv}\frac{dv}{ds}, \tag{2}$$

where $v = v_{LSR}$ is the LSR radial velocity and s is the distance from the Sun. Recalling $N_{H_2} = X_{CO}\int T_B dv$, we have

$$n_{H_2} = X_{CO}T_B(dv/ds), \tag{3}$$

where X_{CO} is the CO-to-H_2 conversion factor assumed to be constant at 2×10^{20} H_2 cm^{-3} [K km s^{-1}]$^{-1}$ (Kohno & Sofue 2023). The velocity gradient, dv/ds, is calculated by

$$dv/ds = (dV/dR - V/R)k\sqrt{1-k^2}, \tag{4}$$

where R is the galacto-centric radius, $V = V(R)$ is the rotation velocity, $k = R_0 \sin l/R$, and v and R are related by $v = (VR_0/R - V_0)\sin l$. We adopt the most accurate rotation curve of the Milky Way (Sofue 2021; Sofue 2023).

Then, we calculate the following values using the LVD:

$$n^*_{HII} = (dN_{HII}/dv)(dv/ds) \tag{5}$$

and

$$n^*_{H_2} = n_{H_2}/X_{CO} = T_B(dv/ds). \tag{6}$$

These quantities are assumed to be proportional to ρ_{SFR} and ρ_{H_2}, respectively, averaged in each bin with size $\delta v_{LSR} \times \delta l$. In order to check the index α, we hereafter investigate the correlation between $\log n^*_{HII}$ and $\log n^*_{H_2}$. Except for the scaling, the plots are equivalent to the KS plot.

Figure 2 shows the thus obtained plots of $\log n^*_{HII}$ against $\log n^*_{H_2}$ averaged in 0.05–0.1 dex bins of the horizontal axes, where the bars are standard errors (SE). We used the data exceeding thresholds of $n^*_{HII} > n^*_{HII;min} = 1$ and $n^*_{H_2} > n^*_{H_2;min} = 0.1$ in order to avoid the lowest-count data. We then determined the KS index α by the least-squares fitting by a linear line in the log-log plane, putting equal weighting to the points, which gave relatively larger weight to high density regions where the number of data points gets smaller so that the SE gets larger. We obtained almost the same results even if we used weights proportional to the inverse of the error bars. The fitting results are shown by the thin lines, and we obtain $\alpha = 1.053 \pm 0.075$ for Nobeyama data in the inner disc at $50° \geq l \geq 10°$ (figure 2, panel A), and 1.031 ± 0.067 for Columbia data in the entire disc avoiding the central region at $|l| \geq 10°$ (panel B). We find nearly equal value $\alpha = 0.905 \pm 0.072$ inside the 4-kpc molecular ring at $30° \geq |l| \geq 10°$ (panel C) for the

Columbia data, and a slightly smaller value 0.892 ± 0.138 outside 4 kpc (panel D).

The Nobeyama data in the GC at $|l| \leq 2°$ (panel A, magenta crosses) show significantly lower number density of HII regions despite much higher gas density, showing an order of magnitude lower efficiency of star formation. Accordingly, the Columbia data in the central region at $|l| \leq 10°$ (magenta crosses and line in panel B), which are mixture of the GC and Galactic disc values, indicate lower HII density but with almost the same index of $\alpha = 0.965 \pm 0.087$. The larger number of data points in panel B despite the narrower longitude range is due to steeply increasing velocity range toward the GC.

We emphasize that the present method uses LVDs directly, not intervened by the sophisticated FOT procedure to convert the radial velocity to the distance, which includes the difficulty to discriminate far- and near-side solutions. Therefore, the measured quantities are more reliable compared to those using the current methods in so far as the power-law index of the KS law is concerned. In table 1 we compare the result with the current determination for the Milky Way and spir and starburst galaxies.

The here obtained volumetric index is slightly larger than that from the current FOT method yielding $\alpha = 0.7$ to 0.8 (table 1 lines 6 and 7). Also, the surface index for the Milky Way lie at slightly larger values of ~ 1.15 (lines 8 to 10). Besides the Milky Way, extensive studies about the KS-law have been obtained in spiral galaxies also indicating mild indices of $\alpha \simeq 0.8 - 1.3$, which are consistent with the present new values. Therefore, we may state that the unity KS-law index is universal. For reference we calculated a simple mean of the listed values except for lines 3 and 4 in table 1 as $\langle\alpha\rangle = 1.048 \pm 0.182$.

On the other hand, a steeper index around $\alpha \sim 1.5$ has been obtained for total gas including HI in galaxies (Kennicutt 1998; Kennicutt & De Los Reyes 2021) and in the Milky Way (Sofue 2017; Sofue 2021). Analysis of the total surface gas density and SFR density from M dwarf stars also yielded $\alpha_{sur} \sim 1.4$ (Fuchs et al. 2009). Also, an even higher values of $\alpha \gtrsim 2$ are reported for the total gas KS law (Boissier et al. 2003; Misiriotis et al. 2006). The difference between the indices of the molecular and total (H_2 +HI) gas KS laws would be due to the intervening phase transition from HI to H_2 , and vice versa. A detailed analysis of the correlation between HI and H_2 will be a subject for a separate paper.
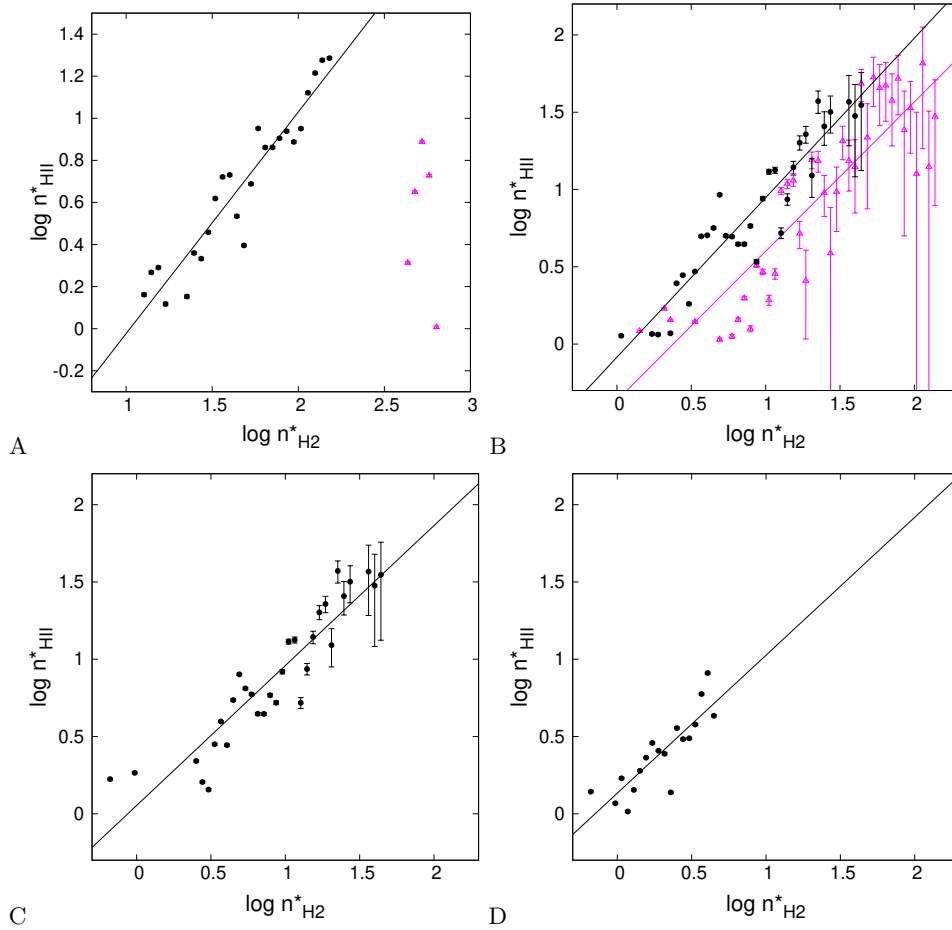
Fig. 2. Plots of log n_{HII}^* using the WISE HII region catalogue against log $n_{\mathrm{H_2}}^*$ using [A] Nobeyama 45-m ^{12}CO data at $|l| = 10° - 50°$ (black dots) and GC $|l| \leq 5°$ (magenta). Grid size is $\delta l \times \delta v = 0.2° \times 10$ km s^{-1}. [B] Same, but using Columbia 1.2 m ^{12}CO at $|l| = 10° - 180°$ (black) and $|l| \leq 10°$ (magenta). Grid size is $2° \times 5$ km s^{-1}. [C] Columbia $|l| = 10° - 30°$ inside 4 kpc. [D] Columbia $|l| = 30° - 180°$ outside 4 kpc. Bars are standard errors in the original scaling data in the 0.05 dex bins of $n_{\mathrm{H_2}}^*$. The straight lines are linear least-squares fit to the log scaling plots with equal weighting.

3 Discussion

3.1 Comparison with KS laws by other methods

The 3D molecular gas maps of the Milky Way derived in our earlier works based on the Columbia CO survey and the Hou's HII region catalogue (Hou et al. 2009) made it possible to measure both the volume and surface densities of the HII regions and molecular gas (Sofue 2017; Sofue & Nakanishi 2017). In these works, we used FOT maps and obtained a smaller slope of $\alpha = 0.78 \pm 0.05$ with log $A = -2.6 \pm 0.05$ for the volume density, while a larger value $\alpha = 1.12 \pm 0.05$ for surface densities. However, a more recent work for the surface-density led to a value closer to unity (Elia et al. 2022). In the meantime during the course to derive face-on molecular gas maps of the inner Milky Way (Sofue 2023) based on the most accurate rotation curve (Sofue 2021), it was shown that the kinematical distance is highly sensitive to the adopted rotation curve. This often results in erroneous maps associated with arti-

fact hole and/or over-condensation of gas near and along the tangent-point circle. It was also shown that the maps are strongly disturbed by the non-circular motion such as due to the 3-kpc expanding ring. Because these problems significantly disturb the KS-law analyses using the face-on maps, we here proposed a more direct method to derive the KS law using the LVDs without employing the FOT.

3.2 Cloud-collision model with $\alpha = 2$

We here consider the cloud collision process and expected KS law. Let the radius of colliding clouds be r_c, number density n_c, and velocity dispersion of the clouds v_c. Then, we have the mean free path

$$l_c = (n_c \pi r_c^2)^{-1} \tag{7}$$

and collision time

$$t_c = l_c / v_c = (v_c n_c \pi r_c^2)^{-1}. \tag{8}$$

The corresponding SFR density is calculated by

Table 1. Molecular-gas KS index α in the Milky Way (first block) compared with those from the literature (following blocks).

Object	Index α	Method[†]	Remarks
Milky Way (this work)			
Inner disc ($|l| = 10°$–$50°$)	1.053 ± 0.075	Vol., LVD, Nobe.45m+WISE[‡]	Fig.2 panel A
Entire disc ($|l| \geq 10°$)	1.031 ± 0.067	Vol., LVD, Col.1.2m+WISE	ibid panel B
Inside 4-kpc* ($|l| = 10°$–$30°$)	0.905 ± 0.072	Vol., LVD, ibid	ibid panel C
Outside 4-kpc* ($|l| > 30°$)	0.892 ± 0.138	Vol., LVD, ibid	ibid panel D
Inside $|l| < 10°$	0.965 ± 0.087	Vol., LVD, ibid	ibid panel B
Milky Way (literature)			
Entire disc	0.78 ± 0.05	Vol., 3D, Col.1.2m+Hou.[†]	(Sofue 2017)
ibid	0.73	Vol. $\rho_{\rm SFR}$	(Bacchini et al. 2019)
ibid	1.12 ± 0.05	Surf. 3D, Col.1.2m+Hou	(Sofue 2017)
ibid	1.14 ± 0.07	Surf., face on	(Elia et al. 2022)
Solar vici. 2 kpc	1.19 ± 0.09	Surf., local clouds & HII	Fit[#] to fig.18 of Spilker et al. 2021
Galaxies (literature)			
NGC/DDO	1.081	Volume	(Kennicutt 1998)
NGC/starburst	1.4 ± 0.15	Surf.	(Kennicutt & De Los Reyes 2021)
NGC/DDO	0.925	Surf.	(Du et al. 2023)
NGC high mol. den.	1.33 ± 0.08	Surf.	(Komugi et al. 2006)
UGC	0.99 ± 0.08	Surf.	(Komugi et al. 2005, 2012)
NGC/IC/Mrk/Arp	1.0	Surf. mol. CO/HCN/IR	(Gao & Solomon 2004)
Disc g's	1.0 ± 0.15	Surf, ALMA CO	(Leroy et al. 2013)
Submm g's	0.81 - 0.84	Surf, sub-mm	(Miettinen et al. 2017)
Interacting g's	1.3 ± 0.04	Surf, CO obs.	(Kaneko et al. 2022)
M83	1.0 ± 0.30	Surf. ALMA CO	Fit[#] to fig.14 of Hirota et al. 2018
Mol. rich galxies	1.07**	Surf, CO, $A_{\rm v}$ cor. Hα	(Wong & Blitz 2002)
Simple mean of all listed α	1.048 ± 0.182	Equal weighting	*Except lines 3, 4 for duplication

[†] Columbia 1.2 m (Dame et al. 2001), Hou et al catalogue (Hou et al. 2009), [‡] Nobeyama 45 m FUGIN and GC surveys (Umemoto et al. 2017; Tokuyama et al. 2019), WISE(Anderson et al. 2014): [#] α of the least squares fit to the plots by log $\Sigma_{\rm SFR} = \alpha$log $\Sigma_{\rm gas}$ with equal weighting. ** Average of 0.78 ± 0.34 with constant $A_{\rm v}$ correction for Hα and 1.36 ± 0.35 with $A_{\rm v}$ proportional to H density.

$$\rho_{\rm SFR} = \eta M_{\rm c} n_{\rm c} t_{\rm c}^{-1} = \pi \eta M_{\rm c} n_{\rm c}^2 r_{\rm c}^2 v_{\rm c} \propto n_{\rm c}^2, \qquad (9)$$

where η is the SF efficiency per one cloud collision and $M_{\rm c}$ is typical mass of molecular clouds [1].

Thus, we obtain $\alpha = 2$, $l_{\rm c} \sim 50$ kpc, $t_{\rm c} \sim 3$ Gy, and $A \sim 10^{-3}\eta$, if we adopt the largest size ($2r_{\rm c} = 5$ pc) of the estimated typical cloud sizes (1 to 5 pc) and collision velocity $v_{\rm c} \sim 15$ km s^{-1}of the estimated 10 to 15 km s^{-1}by the collision hypothesis (Fukui et al. 2021). Here, we assumed $M_{\rm c} \sim 10^{4-5} M_{\odot}$ and $n_{\rm c} \sim (100$ pc$)^{-3}$ referring to the molecular cloud density in the Galactic disc (Solomon et al. 1987). Thus obtained slope does not fit the observation, and the amplitude is too small compared with that in the Milky Way ($A \sim 10^{-3}$), unless an anomalously high SF efficiency of $\eta \sim 1$ is attained.

On the other hand, a number of 'evidences' for cloud collisions are reported (Fukui et al. 2021) (and the literature therein). As to the morphology of cavities in the

---

[1] The same formulation applies to surface density Σ by replacing $\pi r_{\rm c}^2$ by $2r_{\rm c}$, $n_{\rm c}$ by $\Sigma_{\rm c}$, yielding $\Sigma_{\rm SFR} \propto \Sigma_{\rm c}^2$

clouds and position-velocity ridges, we point out that both can be created by an expanding molecular shell driven by an expanding HII region (Sofue 2023). We also mention that unbound two objects moving on hyperbolic orbits rarely collide, unless the angular momentum is removed. There seems no measurement yet about the angular momentum or transverse velocity, line-of-sight distance, and the sense of approaching or receding. Also, the reported mutual velocities, ~ 10–30 km s^{-1}, allow for kinematic distance of ~ 1 kpc between the clouds according to the Galactic rotation. So, some of the evidences seem to be not conclusive yet, leaving room to consider different SF triggering mechanisms.

3.3 Stochastic star formation with $\alpha = 1$

We have shown that the KS-law index of the Milky Way is unity, $\alpha \simeq 1.0$, which prefers the stochastic SF scenario. A possible mechanism for stochastic SF is the self-gravitational contraction of isolated molecular clouds,

which works in the scheme of the sequential star formation (Elmegreen & Lada 1977) and gravitational instability in the hub and filaments (Myers 2009).The growth (Jeans) time of instability in a molecular cloud of density $\sim 10^3 - 10^4$ H$_2$ cm^{-3} is $t_{\rm J} \sim 1/\sqrt{4\pi G\rho} \sim 0.2 - 0.5$ My. If this time is regarded as the SF time, the stochastic SF is more efficient than that presumed by cloud collision time as estimated in the previous subsection.

The global SFR density $\rho_{\rm SFR}$ is proportional to the number density $n_{\rm c}$ of clouds in the averaging bins with $\delta l \times \delta v$, where the shape of the mass function of molecular clouds is assumed to be universal and the Jeans time of individual clouds with the same mass is equal to each other. On the other hand, the probability of SF in each cloud by gravitational collapse depends on the gas density and velocity dispersion inside each cloud, but not on the environment. The SFR density averaged in an area sufficiently wider than clouds' size is, therefore, simply proportional to the number density of clouds, or $\alpha = 1$, which is indeed observed in the present analysis.

3.4 Suppression of SF in the Galactic Centre

Figure 2 showed that the SFR density in the GC is comparable to that in the disc despite the much higher density of molecular gas. This indicates a significantly lower efficiency of star formation, in agreement with the current estimation of an order of magnitude lower star formation efficiency (Kruijssen et al. 2014; Barnes et al. 2017). The SF in the GC is, thus, possibly suppressed by some external actions such as the high magnetic pressure, fast differential rotation with strong shear, turbulence induced by explosive events in the nucleus, and/or external disturbance by falling gaseous debris from the merged companions. We point out that the low SF efficiency (SFE) in the GC despite of the high density and high velocity dispersion does not support the collision scenario.

However, we comment that a possibility cannot be excluded that the apparently low SFE is merely due to the detection limit of the current RRL observations beyond ~ 8 kpc particularly in the GC direction for the high background emission.

3.5 Limitation of the analysis

We used the CO-line LVD along the Galactic plane at $b = 0°$ for the molecular gas in order to represent the densest part of the disc and to avoid the complexity arising from the mixture of gases at different distances and heights. Accordingly, we constrained the HII regions to near Galactic plane objects at $|b| \lesssim 0°.2$, typically $h \lesssim 20$ pc, by which about a half of the catalogued HII regions with RRL velocities was not used. This caused less number of HII regions compared to the current studies, while it avoided the uncertainty arising from the uncertain distances and heights.

Another concern is the incompleteness of the catalogued HII regions caused by the detection limit of the RRL due to decreasing fluxes with the distance. This yields apparently decreasing density of HII regions beyond several kpc (Hou & Han 2014). On the other hand the detection limit of the CO-line does not depend on the distance in so far as the molecular disc is resolved. This situation results in missing HII regions for finite CO intensity regions beyond several kpc, so that the SFR density there is underestimated, and may cause a systematic error in the slope.

We checked this point by dividing the data into different longitudinal ranges, so that they represent data sets with different mean distances from the observer according to the lopsided location of the Sun in the Galaxy. As shown in table 1, we do not find significant dependence of the index on the regions. So, we consider here that the effect is rather even or negligible, not strongly disturbing the general property of KS index. However, in order to ultimately answer this question and the reason for the low SFE in the GC, we may need to wait for an RRL survey sufficiently sensitive to cover the entire Galaxy.

4 Summary

By correlation analysis of the distributions of molecular gas and HII regions in the longitude-velocity diagrams of the Milky Way, we determined the KS index to be $\alpha \simeq 1.0$ in the Galaxy. The index is consistent with those derived in spiral galaxies for molecular gas as listed in table 1. The unity KS index is in favor for the stochastic (spontaneous) star formation by self-regulation in individual molecular clouds, while it contradicts the cloud-collision model. We also suggested that the SFR density in the Galactic Centre may be lower than that in the disc by an order of magnitude, indicating anomalous suppression of SF.

Data availability

The Colombia CO data were retrieved from the URL: https:// lweb.cfa.harvard.edu/ rtdc/ CO/; The WISE HII region catalogue: http:// astro.phys.wvu.edu/wise/; FUGIN Nobeyama CO survey: http://jvo.nao.ac.jp/portal; and GC CO survey: https:// www.nro.nao.ac.jp/ ~nro45mrt/html/ results/data.html

Conflict of interest

There is no conflict of interest.

References

Anderson, L. D., Bania, T. M., Balser, D. S., et al. 2014, ApJS, 212, 1. doi:10.1088/0067-0049/212/1/1

Bacchini, C., Fraternali, F., Iorio, G., et al. 2019, AA, 622, A64. doi:10.1051/0004-6361/201834382

Barnes, A. T., Longmore, S. N., Battersby, C., et al. 2017, MNRAS, 469, 2263. doi:10.1093/mnras/stx941

Boissier, S., Prantzos, N., Boselli, A., et al. 2003, MNRAS, 346, 1215. doi:10.1111/j.1365-2966.2003.07170.x

Dame, T. M., Hartmann, D., & Thaddeus, P. 2001, ApJ, 547, 792. doi:10.1086/318388

Du, K., Shi, Y., Zhang, Z.-Y., et al. 2023, MNRAS, 518, 4024. doi:10.1093/mnras/stac3341

Elia, D., Molinari, S., Schisano, E., et al. 2022, ApJ, 941, 162. doi:10.3847/1538-4357/aca27d

Elmegreen, B. G. & Lada, C. J. 1977, ApJ, 214, 725. doi:10.1086/155302

Fuchs, B., Jahreiß, H., & Flynn, C. 2009, AJ, 137, 266. doi:10.1088/0004-6256/137/1/266

Fujita, S., Ito, A. M., Miyamoto, Y., et al. 2023, PASJ, 75, 279. doi:10.1093/pasj/psac104

Fukui, Y., Habe, A., Inoue, T., et al. 2021, PASJ, 73, S1. doi:10.1093/pasj/psaa103

Gao, Y. & Solomon, P. M. 2004, ApJ, 606, 271. doi:10.1086/382999

Habe, A. & Ohta, K. 1992, PASJ, 44, 203

Hacar, A., Clark, S. E., Heitsch, F., et al. 2023, Protostars and Planets VII, 534, 153. doi:10.48550/arXiv.2203.09562

Hasegawa, T., Sato, F., Whiteoak, J. B., et al. 1994, ApJL, 429, L77. doi:10.1086/187417

Hirota, A., Egusa, F., Baba, J., et al. 2018, PASJ, 70, 73. doi:10.1093/pasj/psy071

Hou, L. G., Han, J. L., & Shi, W. B. 2009, AA, 499, 473. doi:10.1051/0004-6361/200809692

Hou, L. G. & Han, J. L. 2014, AA, 569, A125. doi:10.1051/0004-6361/201424039

Kaneko, H., Kuno, N., Iono, D., et al. 2022, PASJ, 74, 343. doi:10.1093/pasj/psab129

Kennicutt, R. C. 1998, ApJ, 498, 541. doi:10.1086/305588

Kennicutt, R. C. & De Los Reyes, M. A. C. 2021, ApJ, 908, 61. doi:10.3847/1538-4357/abd3a2

Kennicutt, R. C. & Evans, N. J. 2012, ARA&A, 50, 531. doi:10.1146/annurev-astro-081811-125610

Kimura, T. & Tosa, M. 1996, AA, 308, 979

Koda, J., Scoville, N., & Heyer, M. 2016, ApJ, 823, 76. doi:10.3847/0004-637X/823/2/76

Kohno, M. & Sofue, Y. 2023, arXiv:2311.13760. doi:10.48550/arXiv.2311.13760

Komugi, S., Sofue, Y., & Egusa, F. 2006, PASJ, 58, 793. doi:10.1093/pasj/58.5.793

Komugi, S., Sofue, Y., Nakanishi, H., et al. 2005, PASJ, 57, 733. doi:10.1093/pasj/57.5.733

Komugi, S., Tateuchi, K., Motohara, K., et al. 2012, ApJ, 757, 138. doi:10.1088/0004-637X/757/2/138

Kruijssen, J. M. D., Longmore, S. N., Elmegreen, B. G., et al. 2014, MNRAS, 440, 3370. doi:10.1093/mnras/stu494

Lada, C. J. & Lada, E. A. 2003, ARA&A, 41, 57. doi:10.1146/annurev.astro.41.011802.094844

Leroy, A. K., Walter, F., Sandstrom, K., et al. 2013, AJ, 146, 19. doi:10.1088/0004-6256/146/2/19

Marasco, A., Fraternali, F., van der Hulst, J. M., et al. 2017, AA, 607, A106. doi:10.1051/0004-6361/201731054

Miettinen, O., Delvecchio, I., Smolčić, V., et al. 2017, AA, 602, L9. doi:10.1051/0004-6361/201731157

Misiriotis, A., Xilouris, E. M., Papamastorakis, J., et al. 2006, AA, 459, 113. doi:10.1051/0004-6361:20054618

Myers, P. C. 2009, ApJ, 700, 1609. doi:10.1088/0004-637X/700/2/1609

Pineda, J. E., Arzoumanian, D., Andre, P., et al. 2023, Protostars and Planets VII, 534, 233. doi:10.48550/arXiv.2205.03935

Shu, F. H., Adams, F. C., & Lizano, S. 1987, ARA&A, 25, 23. doi:10.1146/annurev.aa.25.090187.000323

Sofue, Y. 2013, PASJ, 65, 118. doi:10.1093/pasj/65.6.118

Sofue, Y. 2017, MNRAS, 469, 1647. doi:10.1093/mnras/stx695

Sofue, Y. 2021, PASJ, 73, L19. doi:10.1093/pasj/psab078

Sofue, Y. 2023, MNRAS, 525, 4540. doi:10.1093/mnras/stad2484

Sofue, Y. 2023, Ap&SS, 368, 74. doi:10.1007/s10509-023-04231-0

Sofue, Y. & Nakanishi, H. 2016, PASJ, 68, 63. doi:10.1093/pasj/psw062

Sofue, Y. & Nakanishi, H. 2017, PASJ, 69, 19. doi:10.1093/pasj/psw123

Solomon, P. M., Rivolo, A. R., Barrett, J., et al. 1987, ApJ, 319, 730. doi:10.1086/165493

Spilker, A., Kainulainen, J., & Orkisz, J. 2021, AA, 653, A63. doi:10.1051/0004-6361/202040021

Tokuyama, S., Oka, T., Takekawa, S., et al. 2019, PASJ, 71, S19. doi:10.1093/pasj/psy150

Umemoto, T., Minamidani, T., Kuno, N., et al. 2017, PASJ, 69, 78. doi:10.1093/pasj/psx061

Wong, T. & Blitz, L. 2002, ApJ, 569, 157. doi:10.1086/339287